PHILOSOPHICAL MAGAZINE B, 1994, VOL. 69, NO. 4, 655–669

Plan-view and profile imaging of sulphided platinum particles

By M. A. GRIBELYUK†, P. J. F. HARRIS‡ and J. L. HUTCHISON

Department of Materials, University of Oxford, Parks Road, Oxford OX1 3PH, England

[*Received 17 June 1993 and accepted 4 October 1993*]

ABSTRACT

Treatment of supported platinum particles with a small concentration of hydrogen sulphide induces {100} faceting, as a consequence of sulphur adsorption. Previous studies have shown that high-resolution electron microscopy is capable of imaging the adsorbed sulphur monolayers directly. Analysis of the profile images observed at the edges of the faceted crystallites has shown that these are apparently consistent with a $c(2 \times 2)$-type monolayer of adsorbed sulphur. However there is clear evidence that the high-resolution images also show the monolayer in transmission, and the interpretation of this contrast has proved less straightforward. The present work describes the plan-view images in more detail and discusses the difficulties in reconciling the transmission contrast with the profile contrast.

§1. INTRODUCTION

High-resolution electron microscopy has great potential for the study of solid surfaces at the atomic level. Two approaches may be used. In the 'profile imaging' technique the surface of interest is aligned parallel to the electron beam and high-resolution images are recorded which show both the bulk structure and a one-dimensional projection of the crystal's edge. This has been employed to image reconstructions in metals (Marks and Smith 1983), as well as the surface structure of complex oxides (Hutchison and Briscoe 1985) and of semiconductors (Gibson, McDonald and Unterwald 1985). Alternatively, plan-view or transmission images of a surface may be obtained by aligning it perpendicular to the incident beam. Plan-view imaging has the obvious advantage of showing the surface in two dimensions, but may not be easy to achieve in practice because contrast from the surface may be swamped by contrast from the bulk. Nevertheless, surface features of (111) gold platelets have been revealed in this way (Nihoul, Abdelmoula and Metois 1984).

The present study involves high-resolution imaging of sulphur monolayers adsorbed on supported platinum particles. Elucidating the structure of such overlayers is of great importance in understanding the way in which sulphur poisons the activity of platinum catalysts. The specimens employed are model catalysts in which the fine platinum particles (mean diameter 10·9 nm) are dispersed over thin films of porous alumina. Sulphidation is carried out by treating the samples with a small concentration of hydrogen sulphide, and results in {100} faceting of the particles (Harris 1986b). These faceted crystallites provide almost ideal candidates for surface-imaging: their near-cubic geometry means that profile and plan-view images may be recorded simultaneously. Previous work on specimens of this type (Jefferson and Harris 1988,

† Present address: Max-Planck-Institut fur Metallforschung, Seestrasse 92 W-7000, Stuttgart 1, Germany.

‡ Present address: Chemical Crystallography Laboratory, University of Oxford, 9 Parks Road, Oxford OX1 3PD, England

0141–8637/94 $10·00

Uppenbrink, Kirkland, Tang and Jefferson 1990) has chiefly concentrated on interpreting profile images of the sulphur monolayer, but there is also clear evidence that the layer can be seen in plan-view. In this work, the contrast observed in the transmission images will be described in more detail and an attempt will be made to develop a model of the overlayer which is consistent with both the plan-view and the profile images.

§2. Experimental procedure

The specimens used in this study consist of self-supporting films of porous γ-alumina over which platinum particles are randomly dispersed. The technique used to prepare the samples has been described fully in previous publications (Harris, Boyes and Cairns 1983, Harris 1986a). Essentially the procedure involves dipping stainless steel microscope grids into an aqueous alumina sol to which a solution of a platinum complex has been added, drying the resultant film to a gel and then firing and reducing this to form thin sheets of catalyst suspended between parts of the grid bars. The films of catalyst are self-supporting and are generally found to be very stable under an electron beam. In the fresh specimens the mean platinum particle diameter is approximately 5 nm. Before treating the samples with sulphur they were heated in air at 700°C to increase the mean particle size to approximately 11·3 nm; surface imaging was found to be easier with these slightly larger particles. Sulphidation was carried out by placing the samples in a controlled atmosphere furnace, flushing with hydrogen, raising the temperature to 500°C and then switching the flow to a mixture of 100 p.p.m. hydrogen sulphide in hydrogen. The flow-rate employed was approximately 10–20 mls min^{-1}. After approximately 20 h the flow was switched back to hydrogen and the samples were cooled. Before opening the apparatus to the atmosphere it was flushed with argon to remove any traces of hydrogen. Oil-free stainless steel valves and regulators were employed and no plastic or rubber components with which the hydrogen sulphide might react were used in the apparatus.

The microscope employed was a JEOL 4000EX with a point-to-point resolution of 0·16 nm, operated at Scherzer defocus with an accelerating voltage of 400 kV. Two different objective apertures were used for the surface imaging, as illustrated in fig. 1. The larger of these (aperture 1) allowed the platinum bulk reflections to contribute to

Fig. 1

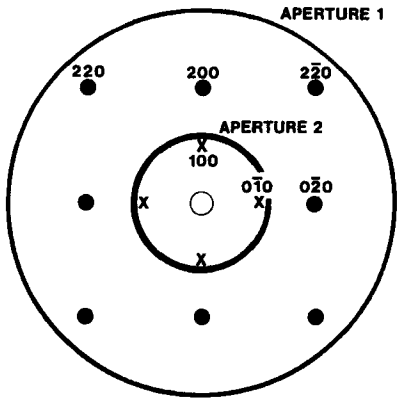

Diagram showing sizes of objective apertures employed in relation to Pt[001] diffraction pattern. Positions of {100} spots are indicated

the image, while aperture 2 blocked all the bulk reflections, allowing only the superlattice to appear in the image. Since the superlattice has a spacing double that of the Pt(200) planes (see below), the superlattice spots would appear at the positions of Pt(100) spots in the diffraction pattern, which are shown in fig. 1. Some low magnification images of general areas were also recorded using a small aperture which blocked all diffracted beams.

§ 3. Image simulations

Multislice image simulations were carried out on an IBM PC AT/386SX microcomputer. In the program employed, the size of a fast Fourier transform (FFT) array must be a power of two, and is calculated from a ratio of lattice parameters in the projection plane. Thus a total number of 16 384 sampling points is maintained. This feature is particularly advantageous if one of the lattice parameters of the extended unit cell is much greater than the other, as is the case for interfaces and profile imaging of particles, for example. Details of the slices used in the simulations are given in the next section.

Elastic absorption was introduced by allowing electron atomic amplitudes, $f(\mathbf{h})$ (where $\mathbf{h}$ is the reciprocal vector), to be complex. Thus, the scattering potential $V(r)$ is

Fig. 2

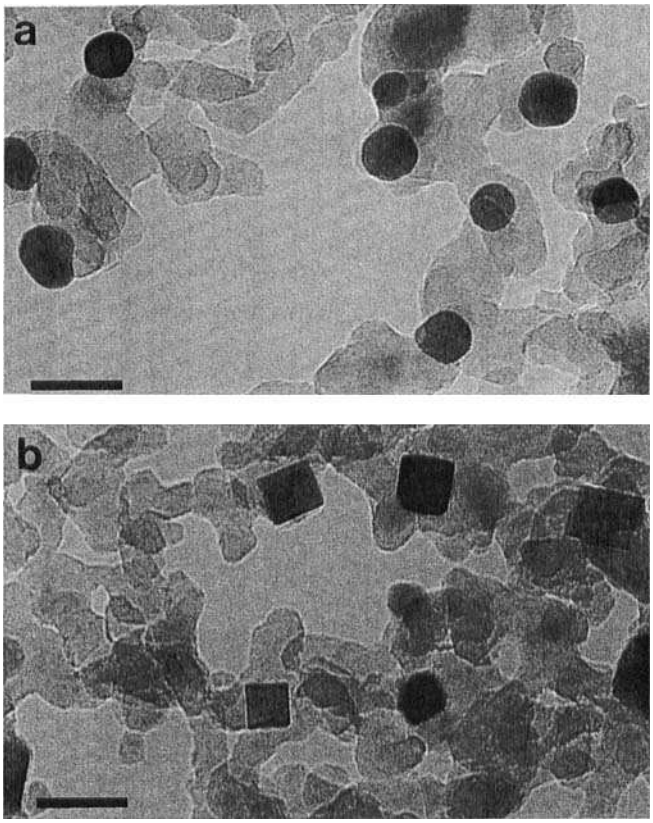

Bright field images showing change in particle shape induced by sulphidation in 100 p.p.m. hydrogen sulphide at 773 K. (*a*) Typical region before sulphidation. (*b*) Sulphided catalyst. Scale bar = 20 nm. Reproduced with permission from 1986, *Nature*, **323**, 792.

also complex with its imaginary part responsible for the decrease in the total intensity of the wave passing through the crystal. Imaginary parts of the electron atomic amplitudes of platinum, $\mathrm{Im}[f_{\mathrm{Pt}}(\mathbf{h})]$, and of sulphur, $\mathrm{Im}[f_{\mathrm{s}}(\mathbf{h})]$, were found in the following way: $\mathrm{Im}[f_{\mathrm{Pt}}(\mathbf{h})]=0{\cdot}1\ f_{\mathrm{Pt}}(\mathbf{h})$ and $\mathrm{Im}[f_{\mathrm{s}}(\mathbf{h})]=0{\cdot}05\ f_{\mathrm{s}}(\mathbf{h})$. The relationship between imaginary and real parts of the electron atomic amplitude is independent of the reciprocal vector $\mathbf{h}$ in this model. In Fourier space, scattering slice potentials have been calculated for all reciprocal vectors $<3\ \text{Å}^{-1}$, providing fine sampling of the slice potential in real space.

§4. Results and discussion

Figure 2 shows the change in particle morphology induced by sulphur adsorption. In a typical specimen prior to sulphidation (fig. 2(*a*)) the particles were generally rounded, with some evidence of {111} faceting. Following sulphur treatment (fig. 2(*b*)), many of the single crystal particles exhibited square or rectangular profiles indicative of {100} faceting. Twinned and multiply twinned particles exhibited more complicated shapes following sulphidation, and these were not examined in this study. It was relatively easy to find a single crystal particle in the correct orientation for surface imaging (i.e. with one of its faces perpendicular to the electron beam), and tilting was not necessary.

A typical high-resolution image recorded with aperture 1 is shown in fig. 3. As in the previous studies (Jefferson and Harris 1988, Uppenbrink *et al.* 1990), a 'castellation' is

Fig. 3

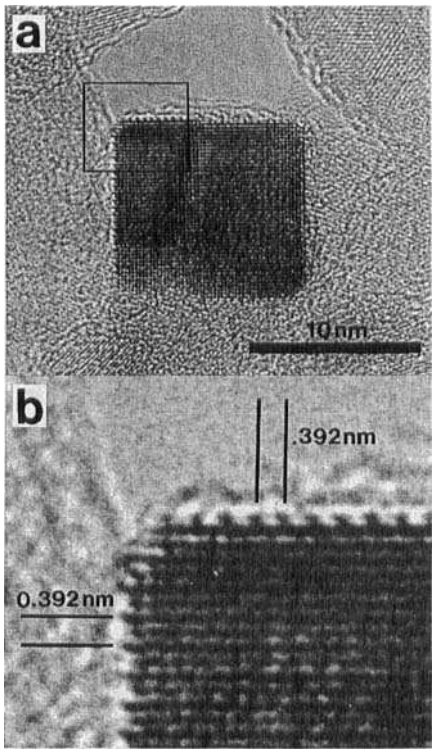

(*a*) High-resolution image of typical sulphided platinum particle, recorded using aperture 1. (*b*) Enlarged area to show detail of profile.

clearly visible along the edges of the particle. The periodicity of this castellation is double that of the Pt(200) spacing, i.e. 0·392 nm, and image simulations show that the contrast is consistent with an adsorbed sulphur monolayer of the $c(2 \times 2)$ type as illustrated in fig. 4. A series of simulated profile images of this surface are given in fig. 5, calculated using the slices shown in fig. 6. It was assumed that the faces of the crystal in the plane of the image were covered with sulphur as well as the faces parallel to the beam, and the slice thickness was 0·196 nm. Thus the top and bottom slices consisted of sulphur atoms only (fig. 6 (*a*)), while the inner slices were alternately platinums only (fig. 6 (*b*)) and platinums with sulphurs at both edges (fig. 6 (*c*)). The total thickness of the crystal was 10·2 nm. It should be noted that these simulations have assumed an adsorption geometry in which the sulphur atoms occupy fourfold surface sites, since Uppenbrink *et al.* (1990) showed that this produced the best agreement with observed images. It can be seen that there is a reasonable agreement between the simulated image at a defocus of -30 nm (fig. 5 (*a*)) and the experimental profile image shown in fig. 3 (*b*).

Fig. 4

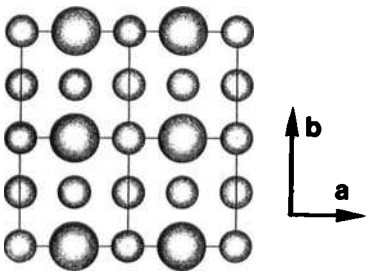

The structure of a $c(2 \times 2)$ sulphur monolayer adsorbed on Pt(001). The large balls represent sulphur, and lines run through atoms which are below the plane of the paper.

Fig. 5

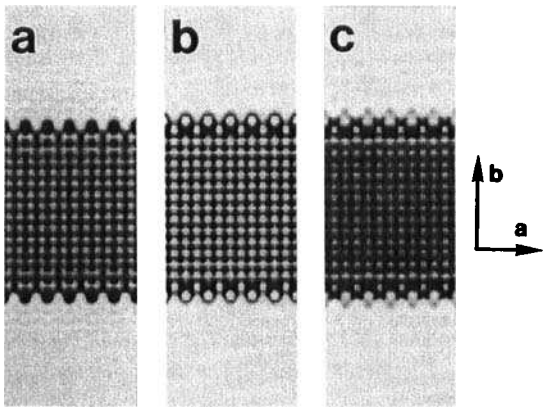

Simulated profile images ((001) projection) of $c(2 \times 2)$S overlayer on Pt(010) and (001) surfaces, assuming a large objective aperture ($R = 7\,\text{nm}^{-1}$). (*a*) Defocus $= -30$ nm, (*b*) -60 nm, (*c*) -70 nm.

Fig. 6

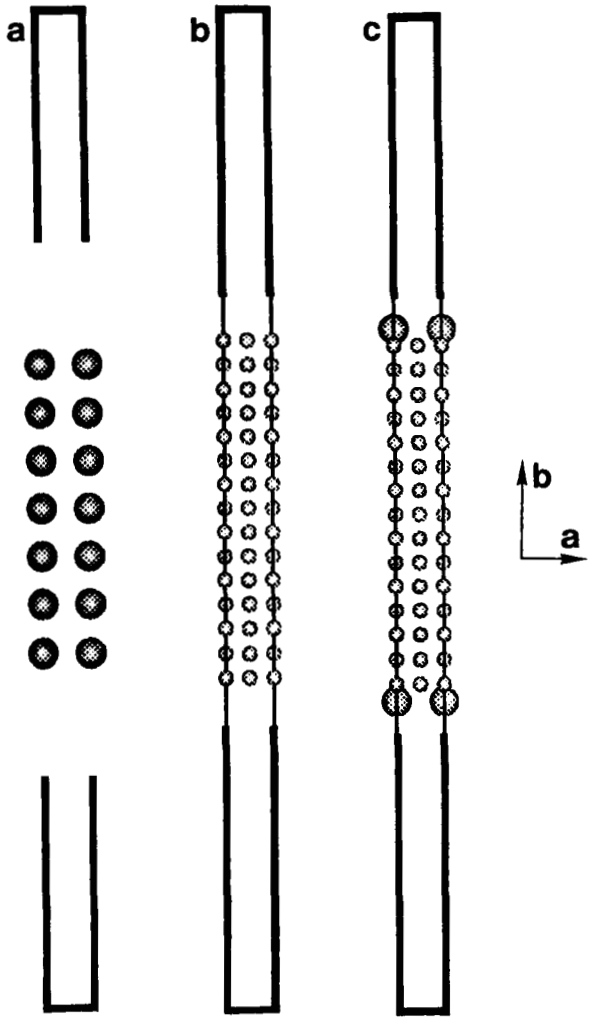

Slices employed in multislice calculations shown in fig. 5; (001) projection. (*a*) Sulphur overlayer on upper and lower faces of crystal. (*b*) Slice made up of seven Pt unit cells. (*c*) Slice with sulphurs at the edges of seven Pt unit cells.

At this defocus the platinum atoms appear as black dots. Figure 7 shows another experimental image exhibiting a 0·392 nm surface periodicity along one of its edges, but in this case the contrast is rather different. Comparison with the simulated images suggests that the defocus here is around −60 nm or −70 nm, with the platinums appearing as white dots.

We consider now the plan-view contrast, which also frequently exhibited evidence of a 0·392 nm periodicity. Figures 8 and 9 show examples of the transmission contrast from two different particles, recorded with aperture 1. In fig. 8 the contrast takes the form of an array of white dots with the 0·392 nm spacing superimposed on the normal Pt(200) square array. In fig. 9, recorded at a different defocus, there are dark lines separating 'blocks' of four light dots. Images recorded with aperture 2, which excluded

Fig. 7

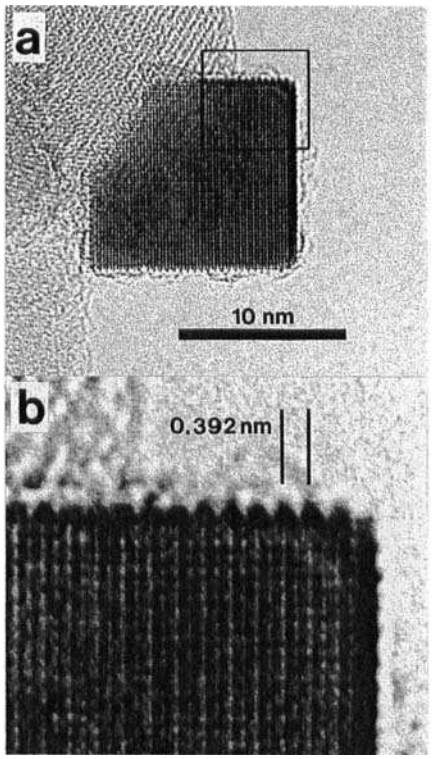

(*a*) High-resolution image (aperture 1) of sulphided platinum particle showing different profile contrast to that displayed in fig. 3. (*b*) Enlarged area showing detail of profile.

all platinum bulk reflections, showed the 0·392 nm spacing even more clearly. This is illustrated in fig. 10, although here a slight misorientation means that the fringes only run in one direction. The appearance of a 0·392 nm periodicity in the plan-view images is surprising, since one would not expect a monolayer of sulphur atoms to be visible against the strong background of a relatively thick platinum crystal. Despite carrying out an extensive series of image simulations using the slices shown in fig. 6, varying the crystal thickness from 1·5 nm to 10 nm, and obtaining a defocus series at each thickness, we were unable to replicate the experimental contrast. The maximum contrast observed in these simulations was 20% for a crystal thickness of 2 nm and a defocus of −30 nm. Although such a contrast level might be visible experimentally, we believe that the crystals are much thicker than 2 nm: tilting experiments suggest an almost cubic shape. For an approximately 10 nm cube, the maximum simulated contrast obtained is only 9%, at a defocus of −50 nm.

Since the experimental plan-view images do not appear to be consistent with an adsorbed $c(2 \times 2)$ monolayer we must consider other possible explanations for the transmission contrast. To begin, we can reject the possibility that the effect may arise from the interface between the platinum particle and the alumina support. It was occasionally possible to find particles which protruded over a hole in the support, and the contrast observed here was identical to that of supported particles. We can also discount the idea that the extra periodicities are due to an incomplete number of

Fig. 8

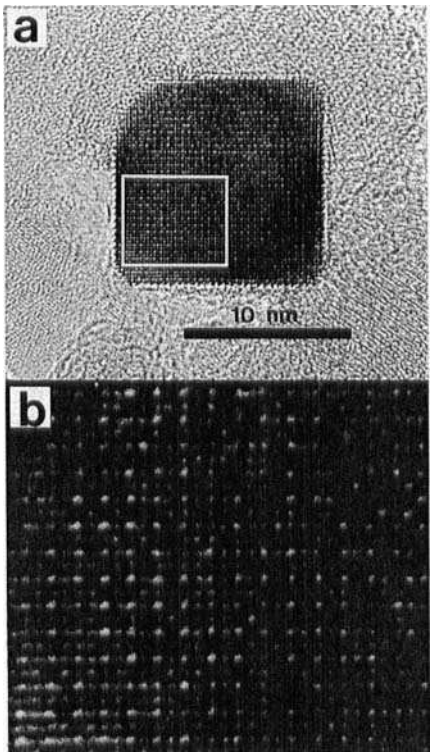

(*a*) High-resolution image of sulphided platinum particle recorded with aperture 1 showing 0·392 nm periodicities in 'bulk' region. (*b*) Enlargement showing nature of the plan-view contrast.

platinum layers. It is well known that diffraction patterns from face-centred cubic (f.c.c.) crystals can sometimes contain 'forbidden' spots if there are an incomplete number of unit cells in the direction of the incident beam. Cherns (1974) used this effect to image surface steps on (111) films of gold. Studies of (100)-oriented gold films by Krakow (1979) have shown that forbidden reflections can also occur in this case, but these are of the (110) type and so could not produce the (100) periodicities observed in the present study. Uppenbrink *et al.* (1990) have suggested that multiple scattering effects could produce the extra (100) periodicities, and have supported this with image simulations. These calculations do indeed indicate that dynamical effects can produce extra contrast in crystals with an incomplete number of layers, but the amount of contrast involved appears to be insignificant compared with that observed experimentally. The failure of Krakow to observe any (100) periodicities in his studies of clean gold films also argues against this idea.

A further possible explanation for the anomalous contrast might be that the particles were tilted slightly away from the true ⟨001⟩ direction. To test this, image simulations were carried out in which the crystal was tilted around the *c* axis in such a way that the (050) diffracted wave propagated along the ⟨001⟩ zone axis (corresponding to a tilt of 10^{-2} rad.), but these did not produce the observed contrast. For completeness, the effect of Fresnel diffraction on the image contrast was also explored. This occurs as a result of the abrupt termination of a crystal producing diffuse

Fig. 9

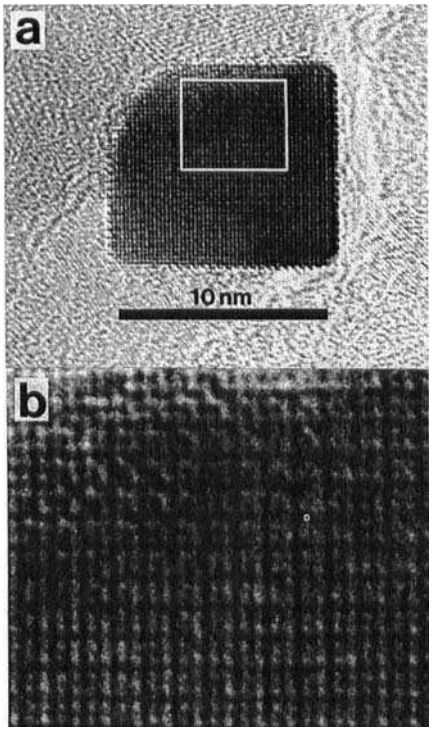

(*a*) Image of similar particle to that shown in fig. 8, also recorded using aperture 1, but with different plan-view contrast. (*b*) Enlarged area.

Fig. 10

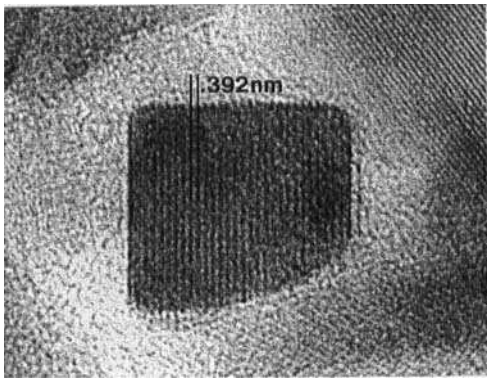

Sulphided platinum particle imaged using aperture 2, so that all Pt bulk reflections are excluded.

continuous scattering in diffraction space. In these simulations the platinum particle was assumed to be infinite in the *a* axis direction, 10·2 nm thick and to consist of seven unit cells in the *b* axis direction (as in fig. 6); an extended unit cell with $a=c=0{\cdot}392$ nm and $b=8{\cdot}14$ nm was employed. The results of some of these simulations are shown in figs. 11 and 12. Figure 11 (*a*) assumes no sulphur overlayer and a small aperture which blocks the {100} reflections. Here relatively strong Fresnel fringes are observed, which fade slightly towards the centre of the crystal. Figure 11 (*b*) again assumes no sulphur layer, but this time the {100} reflections are included. In this simulation the Fresnel fringes are somewhat weaker due to the inclusion of more diffuse scattering as well as the {100} reflections, and calculations show that the intensity decreases markedly as one moves from the edge of the particle towards the bulk. The 'penetration depth' for Fresnel fringes is estimated at 2 nm. In fig. 11 (*c*) a monolayer of sulphur has been placed on the upper and lower surfaces of the platinum crystal (i.e. perpendicular to the beam), assuming a thickness of 9·8 nm. This results in weak {100} lattice fringes. However, when sulphur monolayers are also placed on the two faces parallel to the beam (as is the case in practice), the contrast is quite different (fig. 11 (*d*)). Here one observes an interference pattern caused by size effects and the $c(2\times2)$ overlayers. The Fresnel fringes are non-equidistant and run diagonally across the crystal, fading towards the centre. This bears no resemblance to the experimental contrast. When a larger objective aperture ($R=7\,\text{nm}^{-1}$) is used for the simulations, the Fresnel fringes are much less apparent, as can be seen in fig. 12. For the Pt(001) crystal with no overlayer (fig. 12 (*a*)), the contrast is dominated by the Pt{200} reflections with just a weak bright fringe near the edge. When a $c(2\times2)$ sulphur overlayer is added to the upper and lower faces (fig. 12 (*b*)) there is little change in the image. Adding sulphur monolayers to the faces parallel to the beam (fig. 12 (*c*)) also has little effect on the contrast in the bulk region. The defocus employed in these simulations was -50 nm.

To summarize the above discussion, it seems clear that the transmission contrast cannot arise as a result of an incomplete number of platinum unit cells, from dynamical effects or from crystal tilt and must therefore be a consequence of the adsorbed sulphur monolayer rather than the platinum crystal itself. However the $c(2\times2)$ monolayer

Fig. 11

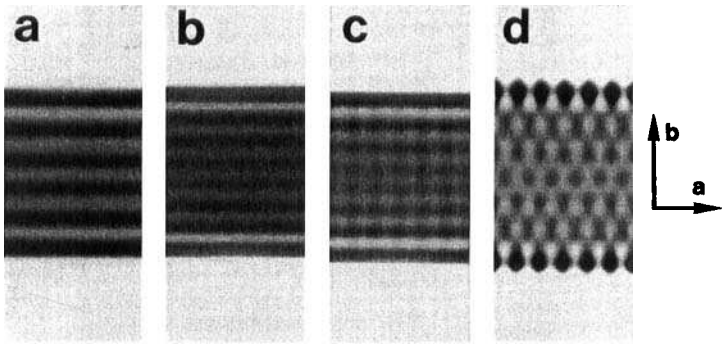

Simulation of Fresnel contrast effects in low-resolution (001) imaging, defocus -40 nm throughout. (*a*) Section of Pt(001) crystal with all reflections excluded by $R=2\,\text{nm}^{-1}$ objective aperture. (*b*) As (*a*), but with larger aperture to include {100} reflections. (*c*) As (*b*), but with top/bottom $c(2\times2)$S overlayers. (*d*) As (*c*), but with $c(2\times2)$ overlayers on edges.

Fig. 12

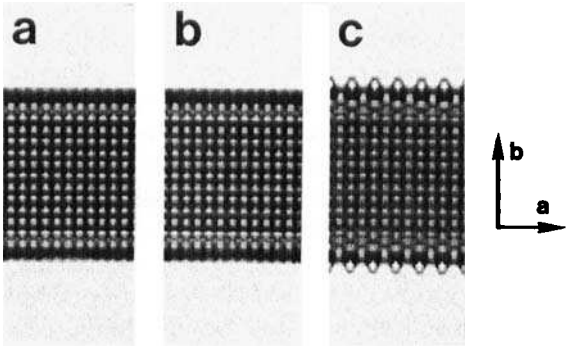

Simulated Fresnel contrast effects in high-resolution (001)imaging ($R = 7\,\mathrm{nm}^{-1}$), with defocus -50 nm. (*a*) Clean Pt(001) crystal. (*b*) Pt(001) with top/bottom $c(2 \times 2)$S overlayers. (*c*) As (*b*) but with $c(2 \times 2)$ overlayers on edges.

produces insufficient contrast to be visible experimentally, and Fresnel contrast effects do not replicate the observed contrast. We are left with the possibility that the $c(2 \times 2)$ structure which we have assumed for the adsorbed sulphur monolayer may be incorrect. With this in mind, we have made a number of attempts to develop an alternative model of the sulphur monolayer which might explain the observed contrast. Of course, any such model must also be consistent with the profile contrast. Initially the effect of varying the adsorption site geometry of the sulphur atoms was explored, but this did not produce significant changes in the predicted transmission contrast. Thus it appeared that substantial disruption of the platinum surface atoms themselves might be required in order to produce the observed contrast. We therefore postulated a model in which the surface effectively comprised a single layer of bulk sulphide rather than a perfect Pt(001) plane with sulphur atoms adsorbed on top. This model is illustrated in fig. 13. Here, sulphur atoms lie below the surface occupying tetrahedral sites within the

Fig. 13

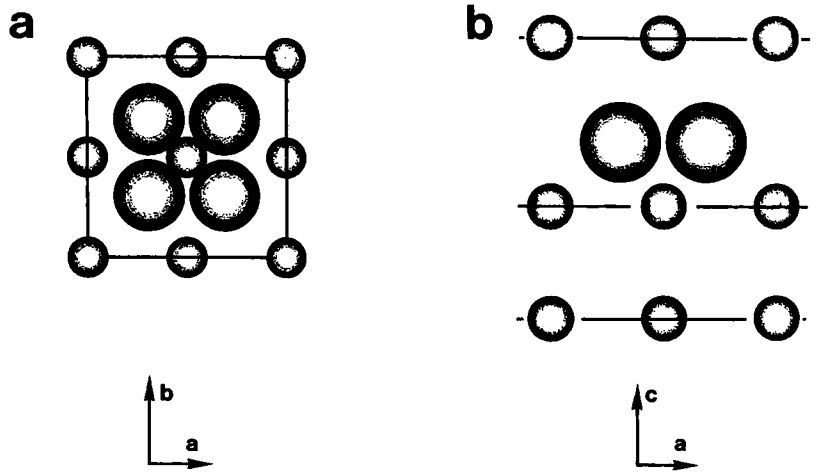

The 'tetrahedral distortion' model of a sulphided platinum (001) surface. (*a*) (001) projection, (*b*) (010) projection. Large balls represent sulphur.

metal f.c.c. lattice, by analogy with the PtS_2 structure (Finley, Schleich, Ackerman, Soled and Wold 1974). In an undistorted lattice the Pt–S separation would be unrealistically small (approximately 0·166 nm), so a tetrahedral distortion is assumed in which the lattice parameter c increases to 0·59 nm, with a and b held at 0·392 nm. This produces Pt–S distances in the range 0·204–0·25 nm. Simulations of the plan-view contrast which this structure would produce were carried out assuming that the top and bottom surfaces consisted of a single layer of the tetrahedrally distorted sulphide structure (fig. 13), with the parameter c set at 0·588 nm. This precise value was chosen as it could be divided into three 0·196 nm thick slices. The inner slices were also 0·196 nm thick and assumed a perfect Pt lattice. These simulations showed that the sulphide surface layers could produce contrast as high as 30% in the plan-view images. Figure 14 shows the transmission contrast for the 'five-beam' case, assuming a defocus of −40 nm. Simulated images for the high-resolution case (objective aperture radius 7 nm^{-1}) are shown in fig. 15. It can be seen that there is a reasonable agreement between the simulated image for a defocus of −30 nm (fig. 15 (*a*)) and the experimental image shown in fig. 8. A contrast reversal occurs for defocii greater than −50 nm.

Profile images for the tetrahedral distortion model were simulated using two different slices. As with the plan-view simulations, the upper and lower faces consisted of single layers of the tetrahedrally distorted structure with $c = 0{\cdot}588$ nm, divided into three slices, while the inner slices assumed a perfect platinum crystal with its (010) edges having the sulphide structure (see fig. 16). An extended unit cell was employed having five platinum unit cells in the b direction. The results of these simulations are given in figs. 17 (for the five-beam case) and 18 (for the high resolution case). None of these simulations closely replicate the experimental profile contrast shown in figs. 3 and 7.

Fig. 14

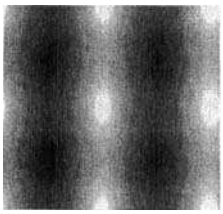

Plan-view five beam (001) image for the tetrahedral distortion model. Defocus −40 nm.

Fig. 15

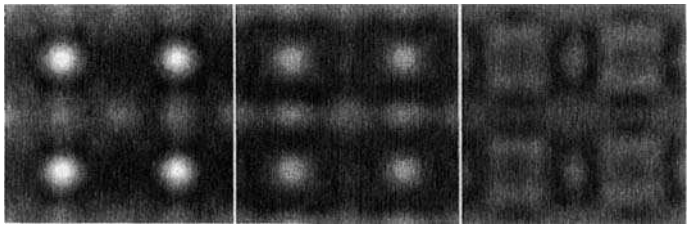

(*a*) (*b*) (*c*)

Simulated high-resolution image for the tetrahedral distortion model. (*a*) Defocus −30 nm, (*b*) −40 nm, (*c*) −60 nm.

Fig. 16

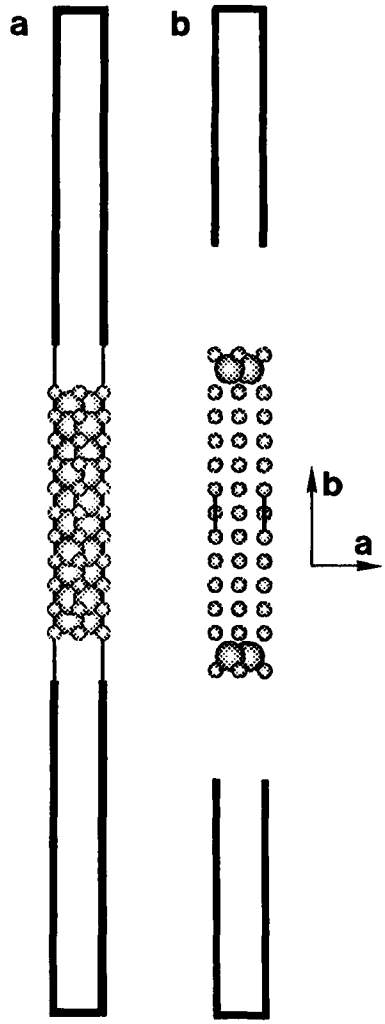

Illustration of the slices used to simulate profile contrast for the tetrahedral distortion model; (001) projection. The upper and lower (i.e. (001)) faces consisted of one layer of the tetrahedrally distorted structure, as shown in (*a*), which was divided into three slices for the simulation. The inner slices were made up of five unit cells of a Pt crystal with both (100) edges having the sulphide structure, as in (*b*).

Fig. 17

The five-beam (001) profile image for the tetrahedral distortion model. Defocus −50 nm.

Fig. 18

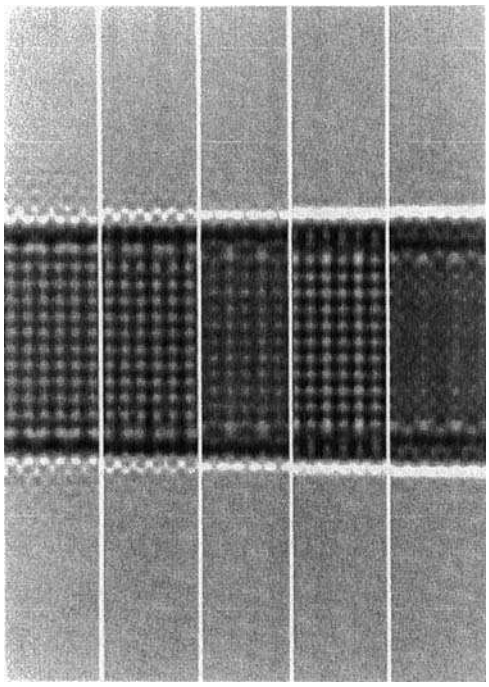

(*a*) (*b*) (*c*) (*d*) (*e*)

High-resolution (001) profile defocus series for the tetrahedral distortion model. (*a*) Defocus −30 nm, (*b*) −40 nm, (*c*) −50 nm, (*d*) −60 nm, (*e*) −70 nm.

§ 5. Conclusions

Despite carrying out extensive image simulations, we have not been able to explain fully the contrast observed in high-resolution images of sulphided platinum particles. The profile images appear to be consistent with a $c(2 \times 2)$ overlayer of adsorbed sulphur atoms, but such a monolayer cannot apparently produce sufficient contrast to be visible in transmission. An alternative model of the surface based on the structure of bulk platinum sulphide produces higher plan-view contrast but little agreement with the profile images. Moreover, this new model does not agree with established models of sulphided platinum surfaces (for example Fischer and Kelemen (1978)). The chief importance of the present work may lie in the demonstration that plan-view imaging of monolayers on the surfaces of relatively thick metal particles is achievable. This suggests that transmission electron microscopy may have significant potential for studying monolayer structures in the plan-view mode, perhaps using thin metal or

semiconductor films upon which adsorbates have been deposited (Marks *et al.* 1991, Xu, Dunn, Zhang and Marks 1993) rather than small metal particles which would not in general have an appropriate geometry.

ACKNOWLEDGMENTS

We thank Professor Sir Peter Hirsch for provision of laboratory facilities and SERC for financial support. One of us (M.A.G.) also thanks the British Council for support during his stay in Oxford. Useful discussions with Dr. D. A. Jefferson of Cambridge University are gratefully acknowledged.

REFERENCES

CHERNS, D., 1974, *Phil. Mag.*, **30,** 549.
FINLEY, A., SCHLEICH, D., ACKERMAN, J., SOLED, S., and WOLD, A., 1974, *Mater. Res. Bull.*, **9,** 1655.
FISCHER, T. E., and KELEMEN, S. R., 1978, *J. Catal.*, **53,** 24.
GIBSON, J. M., MCDONALD, M. L., and UNTERWALD, F. C., 1985, *Phys. Rev. Lett.*, **55,** 1765.
HARRIS, P. J. F., 1986a, *J. Catal.*, **97,** 527; 1986b, *Nature*, **323,** 792.
HARRIS, P. J. F., BOYES, E. D., and CAIRNS, J. A., 1983, *J. Catal.*, **82,** 127.
HUTCHISON, J. L., and BRISCOE, N. A., 1985, *Ultramicroscopy*, **18,** 435.
JEFFERSON, D. A., and HARRIS, P. J. F., 1988, *Nature*, **332,** 617.
KRAKOW, W., 1979, *Ultramicroscopy*, **4,** 55.
MARKS, L. D., AI, R., BONEVICH, J. E., BUCKETT, M. I., DUNN, D., ZHANG, J. P., JACOBY, M., and STAIR, P. C., 1991, *Ultramicroscopy*, **37,** 90.
MARKS, L. D., and SMITH, D. J., 1983, *Nature*, **303,** 316.
NIHOUL, G., ABDELMOULA, K., and METOIS, J. J., 1984, *Ultramicroscopy*, **12,** 353.
UPPENBRINK, J., KIRKLAND, A. I., TANG, D., and JEFFERSON, D. A., 1990, *Surf. Sci.*, **238,** 132.
XU, P., DUNN, D., ZHANG, J. P., and MARKS, L. D., 1993, *Surf. Sci.*, **285,** L479.